JOINT SPECTRAL CLUSTERING AND RANGE ESTIMATION FOR 3D SCENE RECONSTRUCTION USING MULTISPECTRAL LIDAR WAVEFORMS

Yoann Altmann, Aurora Maccarone, Aongus McCarthy, Gerald Buller and Steve McLaughlin†*

School of Engineering, Heriot-Watt University, Edinburgh, U.K.
Email: {Y.Altmann, am827, A.McCarthy, G.S.Buller, S.McLaughlin}@hw.ac.uk

ABSTRACT

This paper presents a new Bayesian clustering method to analyse remote scenes sensed via multispectral Lidar measurements. To a first approximation, each Lidar waveform mainly consists of the temporal signature of the observed target, which depends on the wavelength of the laser source considered and which is corrupted by Poisson noise. By sensing the scene at several wavelengths, we expect a more accurate target range estimation and a more efficient spectral analysis of the scene. Thanks to its spectral classification capability, the proposed hierarchical Bayesian model, coupled with an efficient Markov chain Monte Carlo algorithm, allows the estimation of depth images together with reflectivity-based scene segmentation images. The proposed methodology is illustrated via experiments conducted with real multispectral Lidar data.

***Index Terms*—** Multispectral Lidar, Depth imaging, Bayesian estimation, Markov Chain Monte Carlo, Spectral clustering.

1. INTRODUCTION

Laser altimetry (or Lidar) is an acknowledged tool for extracting spatial structures from three-dimensional (3D) scenes. Using time-of-flight to create a distance profile, signal analysis can recover, for instance, tree and canopy heights, leaf area indices and ground slope by analyzing the reflected photons from a target. Conversely, passive multispectral (MSI) (dozen of wavelengths) and hyperspectral images (HSI) (hundreds of wavelengths) are widely used to extract spectral information about the scene which, for forest monitoring, can also provide useful parameters about the canopy composition and health. The most natural evolution to extract spatial and spectral information from sensed scenes is to couple Lidar data and multi/hyperspectral images [1, 2]. Although the fusion of Lidar data and HSIs can improve scene characterization, data synchronization issues in space (alignment, resolution) and time (dynamic scene, change of observation conditions, etc) are still open issues. For these reasons, multispectral Lidar (MSL) has recently received attention from the remote sensing community for its ability to extract both structural and spectral information from 3D scenes [3–5]. The key advantage of MSL is the ability to provide information on the full 3D distribution of materials, especially for scenes including semi-transparent objects (e.g., vegetation or fences). Another motivation for MSL is that HSI, even when fully synchronized, can only integrate the spectral response along the path of each optical ray, not measure the spectral response as a function of distance, e.g. depth into a forest canopy. In [5–7], spectral unmixing techniques have been developed to analyze 3D scenes composed of multi-layered objects, assuming that the spectral signatures of the materials composing the scenes were known and assuming linear mixing processes. In this paper we assume that for each pixel, the photons emitted by the pulsed laser sources at different wavelength are reflected onto a single surface. This is typically the case for short to mid-range (up to dozens of meters) depth imaging where the divergence of the laser source(s) can be neglected. Moreover, for such applications, the size of the laser beam (i.e., its footprint) projected onto a surface of the scene is generally relatively small (hundreds of microns) yielding a high probability for this surface to be composed of a single material. In a similar fashion to high spatial resolution passive hyperspectral images, in the absence or lack of spectral mixtures, it seems more sensible to use faster classification methods to analyse MSL data. This is precisely the aim of this paper which studies, for the first time to the best of our knowledge, a spectral clustering algorithm for the analysis of MSL data.

Single-photon Lidar and thus MSL systems usually record, for each pixel/region of the scene, a histogram of time delays between emitted laser pulses and the detected photon arrivals. Thus the classical additive Gaussian noise assumption used for passive hyperspectral images is not as suitable and Poisson noise models are more appropriate for sparse photon count MSL signals. Indeed, Within each histogram bin, the number of detected photons follows a discrete distribution which can be approximated by a Poisson distribution due to the particle nature of light. Due to the design of the proposed experiments (performed indoor) and to simplify the estimation problem, we further assume that the ambient light (e.g., solar illumination) and dark counts potentially effecting the recorded the MSL waveforms can be neglected. In this paper, we demonstrate the possibility of efficient 3D scene analysis by exploiting geometric and spectral information contained in MSL data, under favourable observation conditions. However, the proposed method can be easily extended to more difficult observation conditions, as discussed in the conclusions of the paper.

Adopting a Bayesian approach, appropriate prior distributions are chosen for the unknown parameters of the model considered here, *i.e.*, the surface positions, the clustering labels and each class parameters. The joint posterior distribution of these parameters is then derived and a Markov chain Monte Carlo (MCMC) method is used to generate samples according to the posterior of interest. This fully Bayesian approach allows a careful study of the estimation performance (through the derivation of measures of uncertainty). Although very interesting, algorithmic improvement in terms of computational complexity (e.g., using optimization methods) is out of scope of this paper and is worthy of more effort which we will report in future work.

The remainder of the paper is organized as follows. Section 2 introduces the observation model associated with MSL returns for a

*Part of this work was supported by the EPSRC via grants EP/N003446/1, EP/K015338/1, EP/M01326X/1

†Part of this work was supported by the EPSRC via grant EP/J015180/1.

978-0-9928-6265-7/16/$31.00 ©2016 IEEE

single-layered object to be analyzed. Section 3 presents the hierarchical Bayesian model associated with the spectral clustering problem considered and the associated posterior distribution. Section 4 describes the MCMC method used to sample from the posterior of interest and subsequently approximate appropriate Bayesian estimators. Results of experiments conducted on real MSL data are shown and discussed in Section 5 and conclusions are finally reported in Section 6.

2. PROBLEM FORMULATION

This section introduces the observation statistical model associated with MSL returns for a single-layered object which will be used in Section 3 for spectral classification of MSL data. We consider a 4-D array $\mathbf{Y}$ of Lidar waveforms and of dimension $N_{\text{row}} \times N_{\text{col}} \times L \times T$, where N_{row} and N_{col} stands for the number of rows and columns of the regular spatial sampling grid (in the transverse plane), L is the number of spectral bands or wavelengths used to reconstruct the scene and T is the number of temporal (corresponding to range) bins. Let $\mathbf{y}_{i,j,\ell} = [\mathbf{Y}]_{i,j,\ell,t} = [y_{i,j,\ell,1}, \ldots, y_{i,j,\ell,T}]^T$ be the Lidar waveform obtained in the pixel (i,j) using the ℓth wavelength. The element $y_{i,j,\ell,t}$ is the photon count within the tth bin of the ℓth spectral band considered. Let $d_{i,j}$ be the position of an object surface at a given range from the sensor, whose spectral signature (observed at L wavelengths) is denoted as $\boldsymbol{\lambda}_{i,j} = [\lambda_{i,j,1}, \ldots, \lambda_{i,j,L}]^T$. According to [8,9] and assuming that the ambient illumination and dark photon counts can be neglected, each photon count $y_{i,j,\ell,t}$ is assumed to be drawn from the following Poisson distribution

$$y_{i,j,\ell,t} | \lambda_{i,j,\ell}, t_{i,j} \sim \mathcal{P}\left(\lambda_{i,j,\ell} g_{0,\ell}(t - t_{i,j})\right) \tag{1}$$

where $g_{0,\ell}(\cdot)$ is the photon impulse response whose shape can differ between wavelength channels and $t_{i,j}$ is the characteristic time-of-flight of photons emitted by a pulsed laser source and reaching the detector after being reflected onto a target at range $d_{i,j}$ ($d_{i,j}$ and $t_{i,j}$ are linearly related in free-space propagation). Moreover, the impulse responses $\{g_{0,\ell}(\cdot)\}$ are assumed to be known and can usually be estimated during the imaging system calibration.

In this work, we further assume that the spectral signatures of the scene surfaces can be clustered into at most K distinct groups or classes whose means and covariances can differ and where K is a user-defined parameter. Note that due to physical considerations the unknown spectral signatures $\{\boldsymbol{\lambda}_{i,j}\}_{i,j}$ are assumed to be positive.

The problem addressed in this paper consists of jointly estimating the range of the targets (for all the image pixels), of identifying the spectral signatures of each target surface, and of clustering these signatures into K groups whose parameters (e.g., mean and covariance) are unknown. Here the clustering step is achieved by assigning each of the $N_{\text{row}} \times N_{\text{col}}$ pixels a label to spectrally segment the scene regions. The next section studies a new Bayesian model to perform joint target range estimation and unsupervised spectral clustering.

3. BAYESIAN MODEL

3.1. Likelihood

Assuming that the MSL waveforms $\mathbf{y}_{i,j} = \{y_{i,j,\ell,t}\}_{\ell,t}$ of a given pixel (i,j) result from the photons reflection onto a surface associated with the spectrum $\boldsymbol{\lambda}_{i,j}$, the likelihood associated with the pixel (i,j) can be expressed as

$$f(\mathbf{y}_{i,j} | \boldsymbol{\lambda}_{i,j}, t_{i,j}) = \prod_{\ell,t} f_{\mathcal{P}}(y_{i,j,\ell,t}; \lambda_{i,j,\ell} g_{0,\ell}(t - t_{i,j})), \tag{2}$$

when assuming that the detected photon counts/noise realizations, conditioned on their mean in all channels/spectral bands are independent. Considering that the noise realizations in the different pixels are independent, the joint likelihood can be expressed as

$$f(\mathbf{Y} | \boldsymbol{\Lambda}, \mathbf{T}) = \prod_{i,j} f(\mathbf{y}_{i,j} | \boldsymbol{\lambda}_{i,j}, t_{i,j}), \tag{3}$$

where $\boldsymbol{\Lambda} = \{\boldsymbol{\lambda}_{i,j}\}_{i,j}$ and $\mathbf{T}$ is an $N_{\text{row}} \times N_{\text{col}}$ matrix gathering the target ranges.

3.2. Prior distributions

In this work, we do not account for the potential spatial correlations between the target distances in neighbouring pixels of the scene. Thus, each target position is considered as a discrete variable defined on $\mathbb{T} = \{t_{min}, \ldots, t_{max}\}$, such that $1 \leq t_{min} \leq t_{max} \leq T$ (in this paper we set $(t_{min}, t_{max}) = (1, T)$) and assign the target ranges independent priors, i.e., $p(t_{i,j} = t) = \dfrac{1}{T'}, \quad t \in \mathbb{T}$ where $T' = \text{card}(\mathbb{T})$. Note that more informative priors could be used instead to capture potential spatial correlations affecting the range profiles, as in [9] where a *total-variation* (TV) regularization [10,11] promoting piecewise constant depth image was used. However, and as will be illustrated in Section 5, when the number of spectral bands L considered and the number of detected photons are significant, the depth estimation does not require informative regularization (as the L bands are used to estimate $t_{i,j}$). For this reason and for paper length constraints, we simply consider independent uniform priors here.

To encode our prior belief that the spectral signatures in $\boldsymbol{\Lambda}$ can be clustered into K groups, we consider the following mixture of conjugate gamma priors

$$\lambda_{i,j,\ell} | z_{i,j} = k, r_{\ell,k}, \theta_{\ell,k} \sim \mathcal{G}(\lambda_{i,j,\ell}; r_{\ell,k}, \theta_{\ell,k}) \tag{4}$$

where $z_{i,j} \in 1, \ldots, K$ is a discrete label associating the pixel (i,j) with the kth spectral cluster whose mean and covariance are characterized by r_{ℓ,k_ℓ} and θ_{ℓ,k_ℓ}.

When prior information about the K spectral signatures characterized by $r_{\ell,k_{\ell,k}}$ and $\theta_{\ell,k_{\ell,k}}$ is available, it can be introduced through an appropriate prior model. Here, we assume that limited knowledge is available (fixed number of classes K) and to reduce the model complexity, we assume that $r_{\ell,k} = r_k, \forall \ell$, which still allows the prior mean and variance of the reflectivity parameters of each class to vary among the wavelengths. We then consider following prior model

$$r_k \sim \mathcal{G}(r_k; r_0 c_0, 1/c_0), \tag{5a}$$

$$\theta_{\ell,l} \sim \mathcal{IG}(\theta_{\ell,k}; \epsilon, \epsilon), \tag{5b}$$

where (r_0, c_0) and ϵ are fixed hyperparameters which specify the shape of the prior $f(r_k)$ and $f(\theta_{\ell,k})$, respectively. Here we choose $(r_0, c_0) = (1, 10)$ and $\epsilon = 10^{-2}$, yielding weakly informative priors. The hierarchical model (4)-(5) assumes that the spectral signatures within each class share *a priori* similar statistical properties (through r_k and $\theta_{\ell,k}$) while being flexible enough to allow to wide range of positive spectral signatures.

Due to the nature of geometric structures in natural scenes, we can often expect neighbouring surfaces of objects to represent the same spectral signatures. To model this prior belief, we consider a Markov random field as a prior distribution for each label $z_{i,j}$ given its neighbors $\mathbf{Z}_{\mathcal{V}(i,j)}$ ($[\mathbf{Z}]_{i,j} = z_{i,j}$), i.e.,

$f(z_{i,j}|\mathbf{Z}_{\setminus(i,j)}) = f(z_{i,j}|\mathbf{Z}_{\mathcal{V}(i,j)})$, where $\mathcal{V}(i,j)$ is the neighbourhood of the pixel (i,j) and $\mathbf{Z}_{\setminus(i,j)} = \{z_{i',j'}\}_{(i',j')\neq(i,j)}$. More precisely, we consider a Potts-Markov model which been widely used for multidimensional image segmentation (see [12, 13] among others). Given a discrete random field $\mathbf{Z}$ attached to an image with N pixels, the Hammersley-Clifford theorem yields $f(\mathbf{Z}) = \frac{1}{G(\beta)} \exp\left[\beta \sum_{(i,j)} \sum_{(i',j')\in\mathcal{V}(i,j)} \delta(z_{i,j} - z_{i',j'})\right]$, where $\beta > 0$ is the (unknown) granularity coefficient of the Potts model, $G(\beta)$ is a normalizing (or partition) constant and $\delta(\cdot)$ is the Dirac delta function. While several neighborhood structures can be employed to define $\mathcal{V}(i,j)$, the eight pixels structure (or 2-order neighbourhood) will be considered in the rest of the paper.

3.3. Joint Posterior distribution

From the joint likelihood and prior model specified in Sections 3.1 and 3.2, we can now derive the joint posterior distribution for $\mathbf{T}, \mathbf{\Lambda}, \mathbf{Z}, \mathbf{r} = \{r_k\}$ and $\mathbf{\Theta} = \{\theta_{\ell,k}\}$, given the observed waveforms $\mathbf{Y}$ and the value of the fixed hyperparameters $\mathbf{\Phi} = (r_0, c_0, \eta)$. Using Bayes' theorem, and assuming prior independence between $\mathbf{T}$, $\mathbf{\Lambda}$ and $\mathbf{Z}$, the joint posterior distribution associated with the proposed Bayesian model is given by

$$f(\mathbf{T}, \mathbf{\Lambda}, \mathbf{Z}, \mathbf{r}, \mathbf{\Theta}|\mathbf{Y}, \mathbf{\Phi}) \propto f(\mathbf{Y}|\mathbf{T}, \mathbf{\Lambda}, \mathbf{Z}) f(\mathbf{\Lambda}|\mathbf{Z}, \mathbf{\Theta}, \mathbf{r}) f(\mathbf{T}) f(\mathbf{r}, \mathbf{\Theta}|\mathbf{\Phi}) f(\mathbf{Z}) \quad (6)$$

4. ESTIMATION STRATEGY

The posterior distribution (6) models our complete knowledge about the unknowns given the observed data and the prior information available. To perform joint depth estimation and spectral classification of the MSL data, we use the following three Bayesian estimators: 1) the minimum mean square error estimator (MMSE) of the spectral signatures $\widehat{\mathbf{\Lambda}}_{\text{MMSE}} = \text{E}[\mathbf{\Lambda}|\mathbf{Y}, \mathbf{\Phi}]$, 2) the maximum a posteriori (MAP) estimator of target ranges $\hat{t}_{i,j}^{\text{MAP}} = \underset{t_{i,j}}{\text{argmax}} f(t_{i,j}|\mathbf{Y}, \mathbf{\Phi})$ and 3) the MAP estimator of the classification labels $\hat{z}_{i,j}^{\text{MAP}} = \underset{z_{i,j}}{\text{argmax}} f(z_{i,j}|\mathbf{Y}, \mathbf{\Phi})$. Note that we use the classical MAP estimators for the target ranges and pixel labels, as this estimator is particularly adapted to estimate discrete parameters. In order to approximate these estimators of interest, we adopt a fully Bayesian approach and consider a Markov chain Monte Carlo method to generate samples according to the joint posterior (6). More precisely, we use a Metropolis-within-Gibbs sampler to generate sequentially the unknown parameters from their conditional distributions and the samples are then used to approximate the Bayesian estimators of interest (after having discarded the first samples associated with the burn-in period of the sampler). The remainder of this section details the main steps of the proposed sampling strategy.

4.1. Sampling the target ranges

It can be seen from (6) that

$$f(\mathbf{T}|\mathbf{\Lambda}, \mathbf{Z}, \mathbf{Y}) = \prod_{i,j} f(t_{i,j}|\mathbf{\Lambda}, \mathbf{Z}, \mathbf{Y}), \quad \forall t_{i,j} \in \mathbb{T}. \quad (7)$$

Consequently, sampling the target ranges can be achieved by sampling independently each depth parameter from its conditional distribution, i.e., by drawing randomly from $\{t_{min}, \ldots, t_{max}\}$ with known probabilities.

4.2. Sampling the classification labels

In a similar fashion to the target ranges, sampling each label $z_{i,j}$ from its conditional distribution can be achieved by drawing in $\{1, K\}$ with known probabilities. In our experiments we used a Gibbs sampler implemented using a colouring scheme such that many labels can be updated in parallel (9 steps required when considering a 2-order neighbourhood structure).

4.3. Sampling the spectral signatures $\boldsymbol{\lambda}$

By exploiting $f(\boldsymbol{\lambda}_{i,j}|\mathbf{Y}, \mathbf{T}, \mathbf{Z}, \mathbf{r}, \mathbf{\Theta}) = \prod_\ell f(\lambda_{i,j}|\mathbf{Y}, \mathbf{T}, \mathbf{Z}, \mathbf{r}, \mathbf{\Theta})$ and the conjugacy of (3) and (4), sampling the spectral signatures in $\mathbf{\Lambda}$ reduces to sampling from independent gamma distributions with known parameters.

4.4. Sampling the hyperparameters r and $\mathbf{\Theta}$

Using the conjugacy of (4) and (5b), the conditional distribution of each $\theta_{\ell,k}$ is a standard inverse-gamma distribution. Thus, the elements of $\mathbf{\Theta}$ can be sampled independently (and in a parallel manner) from their conditional distributions. Conversely, the conditional distribution of r_k is a non-standard distribution and a Metropolis-Hastings step with Gaussian random walk proposal is used here to update each r_k, in a similar fashion to [14]. Note that $f(r_k|\mathbf{\Lambda}, \mathbf{\Theta}, \mathbf{\Phi})$ is log-concave with $c_0 r_0 > 1$.

Note that a main advantage of Bayesian methods is that they often allow estimation of the appropriate amount of regularisation from data. Indeed, there are several Bayesian strategies for selecting the value of the regularisation parameter β in a fully automatic manner (see [15] for a recent detailed survey on this topic). In this paper we use the empirical Bayes technique recently proposed in [16], where the value of β is calculated by maximum marginal likelihood estimation. For brevity however, we assume β is fixed in the remainder of this paper.

5. RESULTS

We propose comparing the performance of the proposed method to analyze the depth and spectral profiles of a approximately 5×5cm scene (see Fig. 1 (a)) composed of different objects made of Fimo clay and mounted on two tree leaves fixed on a painted backboard at a distance of 1.8m from a time-of-flight scanning sensor, based on time-correlated single-photon counting (TCSPC). The transceiver system and data acquisition hardware used for this work is broadly similar to that described in [9, 17–21], which was previously developed at Heriot-Watt University. The measurements have been performed indoor, in the dark to limit the influence of ambient illumination. The scene has been scanned using a regular spatial grid of 170×180 pixels and $L = 33$ regularly spaced wavelengths ranging from 500nm to 820nm. The histograms consist of $T = 3000$ bins of 2ps, which represents a depth resolution of 300μm per bin. The power of the supercontinuum laser source has been adjusted from preliminary runs and the per-pixel acquisition time is 10ms for each wavelength. The instrumental impulse responses $g_{0,\ell}(\cdot)$ were estimated from preliminary experiments by analyzing the distribution of photons reflected onto a Spectralon panel (a commercially available Lambertian scatterer). The proposed algorithm has been applied with $N_{\text{MC}} = 3000$ sampler iterations, including $N_{\text{bi}} = 1000$ burn-in iterations, which corresponds to a processing time of about 10 minutes for a Matlab R2014a implementation on a i7-3.0 GHz desktop computer (16GB RAM). Fig. 1 ((b) and (c)) depicts examples of classification and range images, estimated with $K = 30$

classes. Note that the marginal posteriors for the depth parameters are concentrated in at most 3-4 consecutive bins (i.e., 0.9 to 1.2mm) for almost all pixels. The results shows that in addition to the objects range estimation, it is possible to discriminate spectrally different surfaces (such as the different shades of green) and identify the regions of the scene where a given material is present (e.g., the green clays #2 and #4). It is interesting to mention that the clustering method is also able to identify significant spectral changes due to the orientation of the surfaces, as can be seen around the corners of the other objects. Note that when increasing K, the additional spectral classes are associated with isolated pixels at the sharp boundaries of the objects. Conversely, decreasing the number of classes tends to merge classes spectrally close (similar means and variances). For completeness, Fig. 2 shows a joint range/spectral classification representation of the 3D-scene including only the 14 main classes of interests.

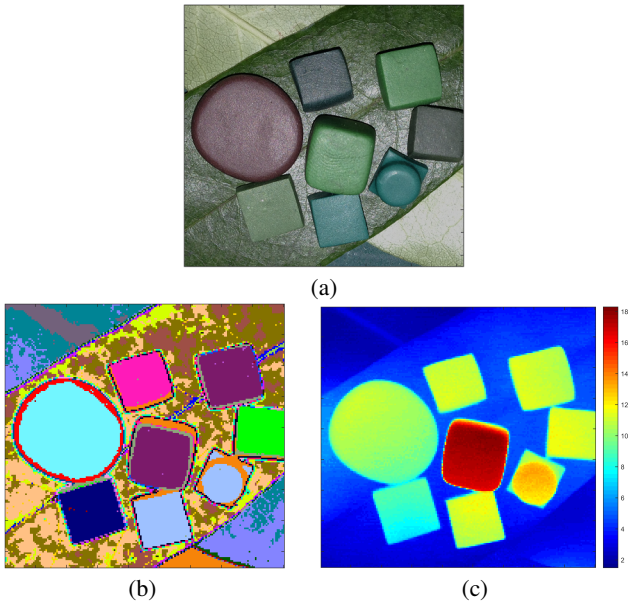

Fig. 1. (a): Standard RGB image of the scene composed of different coloured clays mounted on tree leaves fixed on a green-painted backboard. (b) Estimated spectral classification ($K = 30$ classes associated with different colors). (c) Estimated depth/range image in millimetre (the reference range corresponds to the backboard range)

Fig. 3 depicts the projection of the estimated spectral signatures ($\boldsymbol{\lambda}_{i,j}$) onto the first three principal components of the principal component analysis (PCA). The clusters are identified using the scene colours used in Fig. 1 (b) and Fig. 2. First, this figure shows that the tree leaves and the man-made objects can be clearly discriminated spectrally (clear separation of the corresponding clusters). Second, these results illustrate to ability of the method to identify clusters with significantly different variances (the leaves on the right-hand side present much more spectral variations than the clay-made objects). Finally, Fig. 4 compares the estimated spectra of the most visually similar objects of the scene, namely, the different green clays and the two leaves. This figure clearly illustrate the benefits of using MSL data for 3D scene analysis. Using several wavelengths generally helps estimating the depth profile. For instance, many of the objects of the scene present low reflectivity coefficients between 600 and 700nm. Consequently, the number of detected photons at these wavelengths and associated with these objects are much lower than

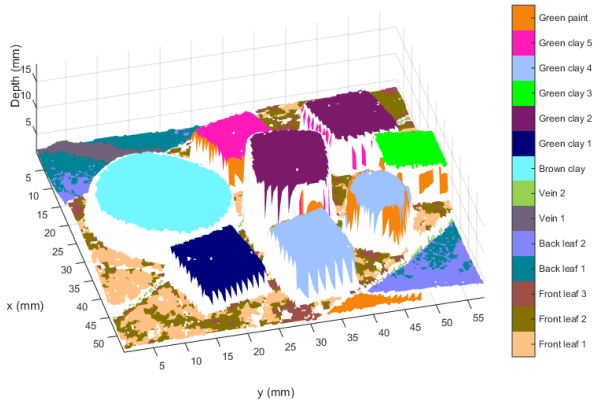

Fig. 2. 3D distribution of the main spectral classes identified by the proposed method ($K = 30$).

at longer wavelengths, which can jeopardize the depth estimation if a single wavelength is used. By splitting the energy of the laser source(s) across several wavelengths, the imaging system becomes more robust to objects that are hardly visible (low reflectivity) at particular wavelengths, which can be useful to reduce acquisition times while preserving imaging performance.

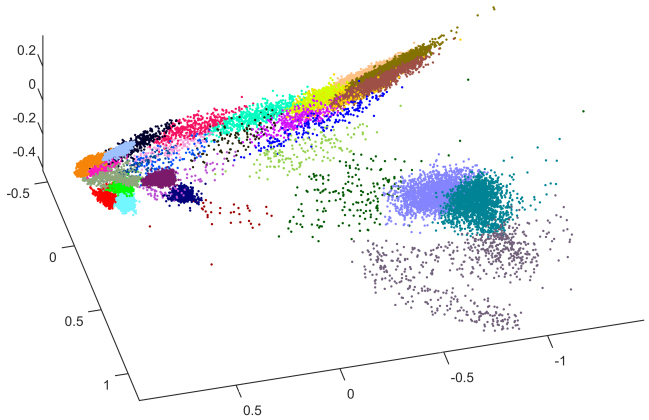

Fig. 3. PCA-based (projection onto the three first principal components) representation of the estimated spectral signatures. The clustering colours corresponds to those used in Fig. 1 (b) and Fig. 2.

6. CONCLUSION

We proposed a new Bayesian model and a joint depth estimation and spectral clustering algorithm for 3D scene analysis from MSL data. Assuming the ambient illumination can be neglected, the scene surfaces visible by the imaging system were clustered into groups sharing the similar spectral signatures. Adopting a Bayesian approach, prior distributions were assigned to the unknown model parameters; in particular, a Potts model was used to model the spatial organization of surfaces in natural scenes. Although it implies a more complex estimation strategy, adjusting the number of classes K and including ambient illumination and dark count levels in the observation model (as in [9, 21–23]) are the obvious next steps for a more general application (especially for long-range imaging applications) of the proposed method. In future work, it would be interesting to

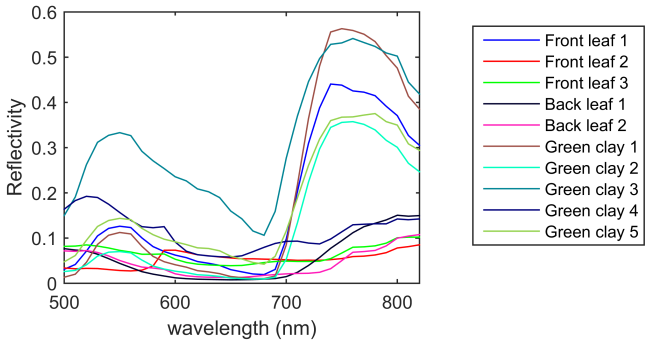

Fig. 4. Estimated spectral signatures of the spectral classes associated with different green clays and the green leaves.

account for the presence of distributed (multi-layered) targets, which would yield multiple returns in the MSL data. Although range-based scene segmentation is out of scope of this paper, coupling spectral and geometric information from the scene (e.g., for multi-layer classification) is a clearly interesting problem.

7. REFERENCES

[1] M. Dalponte, L. Bruzzone, and D. Gianelle, "Fusion of hyperspectral and lidar remote sensing data for classification of complex forest areas," *IEEE Trans. Geosci. and Remote Sensing*, vol. 46, no. 5, pp. 1416–1427, May 2008.

[2] Simon J. Buckley, Tobias H. Kurz, John A. Howell, and Danilo Schneider, "Terrestrial lidar and hyperspectral data fusion products for geological outcrop analysis," *Computers & Geosciences*, vol. 54, no. 0, pp. 249–258, 2013.

[3] A. M. Wallace, C. J. Nichol, and I. H. Woodhouse, "Recovery of forest canopy parameters by inversion of multispectral lidar data," *Remote Sensing*, vol. 4, no. 2, pp. 509–531, 2012.

[4] T. Hakala, J. Suomalainen, S. Kaasalainen, and Y. Chen, "Full waveform hyper-spectral lidar for terrestrial laser scanning," *Opt. Express*, vol. 20, no. 7, pp. 7119–7127, Mar 2012.

[5] Y. Altmann, A. Wallave, and S. McLaughlin, "Spectral unmixing of multispectral lidar signals," *IEEE Trans. Signal Process.*, vol. 63, no. 20, pp. 5525–5534, Oct. 2015.

[6] D. Ramirez, G. S. Buller, A. McCarthy, X. Ren, A. M. Wallace, S. Morak, C. Nichol, and I. Woodhouse, "Developing hyperspectral lidar for structural and biochemical analysis of forest data," in *Advances in Geosciences, Proceedings of EARSEL Conference*, Mykonos, Greece, May 2012.

[7] A. M. Wallace, A McCarthy, C.J. Nichol, Ximing Ren, S. Morak, D. Martinez-Ramirez, IH. Woodhouse, and G. S. Buller, "Design and evaluation of multispectral lidar for the recovery of arboreal parameters," *IEEE Trans. Geoscience and Remote Sensing*, vol. 52, no. 8, pp. 4942–4954, Aug 2014.

[8] S. Hernandez-Marin, A. M. Wallace, and G. J. Gibson, "Bayesian analysis of lidar signals with multiple returns," *IEEE Trans. Patt. Anal. Mach. Intell.*, vol. 29, no. 12, pp. 2170–2180, Dec 2007.

[9] Y. Altmann, X. Ren, A. McCarthy, G. S. Buller, and S. McLaughlin, "Lidar waveform based analysis of depth images constructed using sparse single-photon data," *ArXiv e-prints*, July 2015.

[10] L. I. Rudin, S. Osher, and E. Fatemi, "Nonlinear total variation based noise removal algorithms," *Phys. D*, vol. 60, no. 1-4, pp. 259–268, Nov. 1992.

[11] A. Chambolle, "An algorithm for total variation minimization and applications," *J. of Mathematical Imaging and Vision*, vol. 20, no. 1-2, pp. 89–97, 2004.

[12] Olivier Eches, Nicolas Dobigeon, and Jean-Yves Tourneret, "Enhancing hyperspectral image unmixing with spatial correlations," *IEEE Trans. Geosci. and Remote Sensing*, vol. 49, no. 11, pp. 4239–4247, Nov. 2011.

[13] Y. Altmann, M. Pereyra, and J. Bioucas-Dias, "Collaborative sparse regression using spatially correlated supports - application to hyperspectral unmixing," *IEEE Trans. Image Processing*, vol. 24, no. 12, pp. 5800–5811, Dec. 2015.

[14] M. Zhou, L. A. Hannah, D. B. Dunson, and L. Carin, "Beta-negative binomial process and poisson factor analysis," in *In AISTATS*, 2012.

[15] M. Pereyra, N. Dobigeon, H. Batatia, and J.-Y. Tourneret, "Estimating the granularity coefficient of a Potts-Markov random field within an MCMC algorithm," *IEEE Trans. Image Processing*, vol. 22, no. 6, pp. 2385–2397, June 2013.

[16] M. Pereyra, N. Whiteley, C. Andrieu, and J.-Y. Tourneret, "Maximum marginal likelihood estimation of the granularity coefficient of a Potts-Markov random field within an mcmc algorithm," in *Proc. IEEE-SP Workshop Stat. and Signal Processing*, Gold Coast, Australia, July 2014.

[17] A. McCarthy, R. J. Collins, N. J. Krichel, V. Fernández, A. M. Wallace, and G. S. Buller, "Long-range time-of-flight scanning sensor based on high-speed time-correlated single-photon counting," *Appl. Opt.*, vol. 48, no. 32, pp. 6241–6251, Nov. 2009.

[18] N. J. Krichel, A. McCarthy, and G. S. Buller, "Resolving range ambiguity in a photon counting depth imager operating at kilometer distances," *Opt. Express*, vol. 18, no. 9, pp. 9192–9206, April 2010.

[19] A. M. Wallace, J. Ye, N. J. Krichel, A. McCarthy, R. J. Collins, and G. S. Buller, "Full waveform analysis for long-range 3d imaging laser radar," *EURASIP Journal on Advances in Signal Processing*, vol. 2010, no. 1, pp. 896708, 2010.

[20] A. McCarthy, X. Ren, A. Della Frera, N. R. Gemmell, N. J. Krichel, C. Scarcella, A. Ruggeri, A. Tosi, and G. S. Buller, "Kilometer-range depth imaging at 1550 nm wavelength using an InGaAs/InP single-photon avalanche diode detector," *Opt. Express*, vol. 21, no. 19, pp. 22098–22113, Sept. 2013.

[21] Y. Altmann, X. Ren, A. McCarthy, G. S. Buller, and S. McLaughlin, "Target detection for depth imaging using sparse single-photon data," in *Proc. IEEE Int. Conf. Acoust., Speech, and Signal Processing (ICASSP)*, Shanghai, China, 2016, to appear, technical report available online, http://yoannaltmann.weebly.com/publications.html.

[22] A. Kirmani, D. Venkatraman, D. Shin, A. Colao, F. N. C. Wong, J. H. Shapiro, and V. K. Goyal, "First-photon imaging," *Science*, vol. 343, no. 6166, pp. 58–61, 2014.

[23] Dongeek Shin, A. Kirmani, V.K. Goyal, and J.H. Shapiro, "Computational 3d and reflectivity imaging with high photon efficiency," in *Proc. IEEE Int. Conf. Image Processing (ICIP)*, Oct. 2014, pp. 46–50.